Interphase-assisted suppression of electrode polarization in nanoparticulate-elastomeric composites *⊙*

A. Barhoumi Meddeb 2 0; Z. Ounaies 0



J. Appl. Phys. 133, 155106 (2023) https://doi.org/10.1063/5.0141243





CrossMark

Articles You May Be Interested In

Extreme enhancement and reduction of the dielectric response of polymer nanoparticulate composites via interphasial charges

Appl. Phys. Lett. (June 2014)

Structurally inhomogeneous nanoparticulate catalysts in cobalt-catalyzed carbon nanotube growth

Appl. Phys. Lett. (August 2014)

Influence of interface roughness on the performance of nanoparticulate zinc oxide field-effect transistors

Appl. Phys. Lett. (August 2008)









Interphase-assisted suppression of electrode polarization in nanoparticulate-elastomeric composites

Cite as: J. Appl. Phys. 133, 155106 (2023); doi: 10.1063/5.0141243 Submitted: 4 January 2023 · Accepted: 1 April 2023 ·

Published Online: 21 April 2023

A. Barhoumi Meddeb^{a)} o and Z. Ounaies



AFFILIATIONS

Department of Mechanical Engineering, and Materials Research Institute, The Pennsylvania State University, University Park, Pennsylvania 16802, USA

^{a)}Author to whom correspondence should be addressed: aum33@psu.edu

ABSTRACT

The electrical properties of polymer nanocomposites are governed by the behavior of the internal charges. In particular, the interphase around the nanoparticles strongly influences the distribution and mobility of charge carriers within the nanocomposites, which, in turn, impacts the performance of these materials. In this work, we probe the internal charge behavior in the presence of nanoparticles with a significant to the presence of these materials. focus on the low-frequency regime using a suite of techniques. By investigating the depolarizing currents and the dependence of the dielectric properties on the frequency and temperature, we demonstrate that the interphases redistribute the space charges, increase their trap depth, and suppress the electrode polarization in an elastomeric nanocomposite. Additionally, we study the effect of the nanoparticle content on the dielectric behavior by comparing the internal charge behavior of 1, 2, and 4 vol. % nanocomposites. At only 4 vol. % loading, the mobility of charge carriers is effectively limited, leading to lower dc conductivity compared to the unfilled elastomer, and 1 and 2 vol. % nanocomposites. These findings are based on the model materials used in this study, TiO2 nanoparticles and polydimethylsiloxane, and can be extended to other nanoparticulate-filled elastomer composites to design lightweight dielectrics, actuators, and sensors with improved capabilities. Judicious manipulation of interfacial phenomena in polymer nanocomposites—especially those with a dilute content of nanoparticles—provides a promising path forward for the design of materials with exceptional electrical and other physical properties.

Published under an exclusive license by AIP Publishing. https://doi.org/10.1063/5.0141243

I. INTRODUCTION

Much of the research in nanoparticulate-modified polymers has focused on the important gains in mechanical properties, where the significant role of the interphase is usually stated as the reason for the improved properties. ¹⁻⁹ For example, Zhao *et al.* and Sun et al. investigated the mechanical properties of epoxy with different nanoparticles and using various chemical treatments. 1,2 Zhao et al. showed an improvement in both Young's modulus and ductility by chemically functionalizing alumina nanoparticles compared to the unfilled epoxy and nanocomposite with untreated particles. Similarly, Sun et al. found that the tensile strength and the toughness were increased for Fe₂O₃-epoxy when the surface of the nanoparticles was chemically functionalized compared to the unfilled epoxy.² In both studies, the toughening of the epoxy in the presence of chemically treated nanoparticles was attributed to the interphase. The authors claim that the interphase contributed to an increase in the dissipation energy during fracture, with increased crack deflection compared to the unfilled epoxy and the composite with untreated nanoparticles. Similarly, interesting interfacial effects have been observed in the dielectric behavior of polymer nanocomposites. 10-20 For example, in their recent review, Luo et al. discussed how the interphase can affect the distribution and motion of space charges in the nanocomposites by creating traps, changing the trap depths, and acting as scattering points, with a positive impact on the polarization and electrical conductivity of the nanocomposites. 10 Carroll et al. showed significant changes in the secondary relaxation peaks of the dielectric spectra, in both the peak shape and the peak position, with the addition of silica nanoparticles to poly(vinyl acetate). They pointed to polymer chain dynamics in the interphase as the mechanism responsible for the observed changes. ¹⁴ Klonos et al. investigated the interfacial effects on the segmental mobility of semicrystalline polydimethylsiloxane

(PDMS) as the matrix in nanocomposites using thermal and dielectric measurements. 19,20 They found that the presence of the nanoparticles suppressed the crystalline phase formation and reduced the mobility of the elastomer chains in the interphase. Theoretical studies have also investigated the effects of the interphases on the properties of polymer nanocomposites and have predicted the significant role that the interphase may play in determining the nanocomposites' behavior. These studies include modeling and analytical calculations, such as molecular dynamics, 21,22 Havriliak-Negami analysis, 23 density functional theory (DFT) calculations, ²⁴ and homogenization methods. ^{25–27} Liu *et al.* used DFT simulations to estimate a dipole moment in barium titanate-Vinylidene fluoride-trifluoroethylenechlorofluoroethylene terpolymer [BTO-P(VDF-TrFE-CFE)]. This induced dipole moment, induced at the interphase between the nanoparticles and the paraelectric polymer, resulted in a ferroelectric behavior in the nanocomposite.²⁴ In our own work, we combined the experimental and theoretical methods to demonstrate that the manipulation of interfacial charges, via particle surface treatments, for example, provides a promising path for the design of materials with exceptional dielectric, mechanical, and coupled properties.^{25,26} We investigated the effects of the interphase on the dielectric properties²⁵ and the mechanical properties²⁶ of polydimethylsiloxane (PDMS) at low loadings of TiO2 nanoparticles. With a focus on the mechanical properties, we determined the presence of three different PDMS phases in the nanocomposites, which exhibited different properties than those of the control PDMS. These phases, from closest to furthest from the nanoparticles, are (1) "occluded" PDMS, where the chains are constrained within the nanoparticle agglomerates, (2) "interfacial" PDMS, where the elastomer chains surround the agglomerates, forming a layer much stiffer than those chains further from the particles, and (3) "bulk" PDMS where chains have higher mobility.

Building further on our work and the literature discussed above, in this paper, we study the behavior of the internal charges and the dielectric relaxations of TiO2-PDMS nanocomposites at three low loadings (1, 2, and 4 vol. %) and compare them to the control PDMS. The goal of this study is to advance the understanding of the effects of the interphase on the macroscopic dielectric properties and relate those effects to the nano- and microscale properties.

Our experimental approach combines dielectric spectroscopy and thermally stimulated depolarization current (TSDC) techniques together with transmission and scanning microscopy as well as measurements of the degree of cross-linking in the elastomeric matrix. We demonstrate that with the higher volume content of interphases at 4 vol. % loading, the electrode interfacial polarization was suppressed, and the low-frequency losses were decreased by redistributing the charges and inhibiting their mobility. Additionally, we determine that the interphases in the 4 vol. % nanocomposite acted as anchoring agents, leading to the highest degree of cross-linking. We selected PDMS as the matrix material because (i) it is a versatile elastomer that affords control over its curing kinetics, including the availability of cross-linking agents, which respond to thermal energy, (ii) it is available in a wide range of molecular weights, and (iii) it has shown potential for applications in new high-end technologies such as artificial muscles and energy harvesters. ^{28–31} For the nanoparticles, TiO₂ is selected because (i) it is a representative hard filler dielectric that (ii) is amenable to in situ synthesis through solgel, (iii) it is available commercially in a wide range of equiaxed sizes from nano to micro, and (iv) the presence of OH groups on its surface facilitates a number of chemistries for functionalization, which is key to controlling dispersion. 32,33 Although the model materials investigated here are TiO2 nanoparticles and Sylgard 184 PDMS, these findings can be extended to other nanoparticulate-filled elastomer composites to design lightweight dielectrics, actuators, and sensors with improved capabilities.

II. MATERIALS AND EXPERIMENTS

Sylgard 184 was used as the PDMS elastomer kit in this study, and it was purchased from Dow Corning. It consists of two parts, a base and a hardener, used at a weight ratio of 9:1. Anatase TiO2 nanoparticles, 15 nm diameter, were acquired from NanoAmor. N-heptane, purchased from Sigma-Aldrich, was used as a solvent, at a base-to-solvent ratio of 5:1 by weight, to reduce the viscosity of the solution and improve the dispersion of the nanoparticles. More details on particles' dispersion can be found in Ref. 26. All the produced films were cured at 120 °C for 6 h, and then, any residual solvent was removed by applying vacuum for 6 h at 120 °C. Three nanocomposites were fabricated at 1, 2, and 4 volume percent (vol. %). The thickness of the resulting films was uniform but varied from 160 to 350 um for the different films.

The equilibrium swelling experiment used toluene as the solvent with five samples from each film. The cut samples were first weighed (between 0.10 and 0.35 g), and then, each sample was submerged in a 20 ml vial filled to ¾ with toluene for 5 days. The weights of the swollen samples were measured on days 4 and 5 with no statistically significant change, indicating that the equilibrium was reached. Then, the swollen samples were dried first at $\frac{\varphi}{2}$ room temperature under vacuum. The dried samples' weights were recorded in intervals of 24 h of drying until no change was observed in the measured values. The equilibrium degree of swelling Q, the average molecular weight between cross-links M_c , and the cross-linking density v were calculated using Eqs. (1)–(4) following the procedure described in Ref. 34,

$$Q = \frac{m_{dry}/\rho_p + (m_{sw} - m_{dry})/\rho_s}{m_{dry}/\rho_p},$$
 (1)

where m_{dry} and m_{sw} are the dried and swollen weights of the sample, respectively, and ho_p and ho_s are the densities of the polymer and the solvent, respectively,

$$M_c = -\frac{\rho_p V_s \left(\phi^{\frac{1}{5}} - \frac{2\phi}{f}\right)}{Ln(1-\phi) + \phi + \chi \phi^2},\tag{2}$$

where V_s is the molar volume of the solvent (106.2 cm³/mol), ϕ is the volume fraction of the elastomer in the equilibrium swollen state $(\phi = 1/Q)$, f is the functionality of the cross-link (f = 4 in this)case), 34,35 and χ is the dimensionless Flory-Huggins polymer -solvent interaction parameter given by the following equation:

$$\chi = 0.459 + 0.134\phi + 0.59\phi^2. \tag{3}$$

The cross-linking density v (in mol/cm³) can then be calculated from the average molecular weight between cross-links M_c (in g/mol)

$$v = \frac{\rho_p}{M_c}. (4)$$

For the electrical measurements, impedance spectroscopy, and thermally stimulated depolarization currents (TSDCs), a 2-cm diameter electrode was applied to both sides of each sample using gold leaves. Impedance spectroscopy was carried out using a Modulab XM MTS system at frequencies ranging from 0.01 Hz to 100 kHz. The temperature was increased from 25 to 150 °C at a step of 25°. DC conductivity, σ_{DC} , at different temperatures was taken as the electrical conductivity of the low-frequency plateau. TSDC technique works by applying a DC electric field, E_p, to the sample at a temperature, T_p , higher than T_g , for a duration t_p . Then, while the electric field is still applied, the temperature is quickly dropped to below T_p . Once the temperature is stabilized, the electric field is turned off and the temperature is increased at a selected rate, β , while the depolarization current is recorded. For this study, TSDC tests were performed using a computer-controlled home-built system consisting of a 4140B pA meter/DC voltage source, a Trek amplifier, a Keithley multimeter, an oven, and a K-type thermometer. Two polarizing fields were used in this study: 7.5 and 15 MV/m. The sample was first poled at 55 °C for 5 min. Then, the temperature was decreased to -140 °C at a cooling rate of 15 °C/min. After 2 min, the electric field was turned off, the sample was short-circuited for about 20 s to dissipate the stray charges, then the temperature was increased at a 7 °C/min rate up to 130 °C, and the discharged current was measured. Three samples were tested for each film to ensure measurements' repeatability.

The nanocomposites were imaged at the microscale with a Verios G4 SEM and at the nanoscale with a Philips 420 TEM.

III. RESULTS AND DISCUSSIONS

Impedance spectroscopy provides insight into the interfacial effects on the dielectric behavior of the nanocomposites over a wide range of frequencies and temperatures. Figure 1 shows the dielectric permittivity (ε_r), dielectric loss (ε''), and electrical conductivity (σ') of the unfilled PDMS and the nanocomposites at 25 and 150 °C. As shown in Fig. 1(a), at 25 °C, the dielectric permittivity moderately increased as the nanoparticle content increased from 1 to 4 vol. %. The dielectric loss, Fig. 1(c), also increased with the addition of the nanoparticles at frequencies above 0.1 Hz. Below 0.1 Hz, the dielectric loss of the 4 vol. % nanocomposite was lower than that of unfilled PDMS. At the higher temperature, the unfilled PDMS, and 1 and 2 vol. % nanocomposites exhibited a significant increase in the dielectric permittivity and loss as the frequency decreased, as shown in Figs. 1(b) and 1(d). The dependence of the dielectric permittivity and dielectric loss on the frequency can give insight into the dominant contributions to the dielectric behavior, distinguishing between dc conductivity and electrode polarization, for example.³⁶ Looking first at unfilled PDMS, at 150 °C, the dielectric permittivity as a function of frequency had three slopes [Fig. 1(b)], given as follows:

(1) In the higher frequency range, between 100 kHz and 10 Hz, the dielectric permittivity had limited frequency dependence.

- (2) From 10 to 0.1 Hz, the dielectric permittivity started increasing as the frequency decreased. This first increase in the slope is due to dc conductivity contributions, which is also indicated by the slope of -1 of the dielectric loss vs the frequency in the log scale, $\log(\varepsilon'')$ vs $\log(f)$.³⁶
- (3) In the lower frequency range, 0.1–0.01 Hz, the dielectric permittivity slope further increased, which corresponds to additional contributions from electrode polarization.³⁶

The 1 and 2 vol. % nanocomposites exhibited similar dielectric behavior as unfilled PDMS with contributions from dc conductivity and electrode polarization to the dielectric response. The 4 vol. % TiO₂ nanocomposite had the lowest dielectric losses at low frequency compared to the other samples. The slope of the dielectric loss as a function of frequency $[\log(\varepsilon'') \sim -\log(f)]$ indicates that the dc conductivity contributions were still present in the 4 vol. % nanocomposite. However, the independence of the dielectric permittivity of the low frequencies for the 4 vol. % nanocomposite indicates the absence of electrode polarization. To summarize, unfilled PDMS, and 1 and 2 vol. % nanocomposites exhibited contributions from electrode polarization and dc conductivity to their dielectric behavior, while the electrode polarization was suppressed in the dielectric response of the 4 vol. % nanocomposite, especially at higher temperatures. The dielectric spectroscopy results are showing the evidence of changes in the internal charges behavior as the nanoparticles content increased, namely, the suppression of charges with 4 vol. % loading of the nanoparticles. The factors that drive the behavior of a composite are the properties of the components and the interactions between them. From the internal charge behaviors exhibited by the nanocomposites investigated in this study, we can state that the noticeably different properties with 4 vol. % loading cannot be solely attributed to the nanoparticle of properties. With the increase in the nanoparticles' content, the interphase volume fraction increases, and its contribution to the effective properties becomes more dominant. One possible reason for the suppression of charges is if the mobility of the charge is hindered by an increase in the cross-linking density of the elastomer. 37,38 In addition, the presence of the nanoparticles and their interphase might lead to changes in the cross-linking density of the elastomeric matrix. To probe this hypothesis, the equilibrium degree of swelling (Q) and the cross-linking density (M_c) were calculated for the nanocomposites and unfilled PDMS using an equilibrium swelling experiment. The experimental procedure and the equations to calculate Q and M_c are detailed in Sec. II. As shown in Table I, the 1 and 2 vol. % nanocomposites had a higher equilibrium degree of swelling, i.e., a lower cross-linking density, than unfilled PDMS. The nanoparticles at the lower contents interfered with the elastomer's cross-linking during the curing process. However, the 4 vol. % loading of nanoparticles increased the crosslinking density compared to unfilled PDMS. There are possibly competing factors in the way the nanoparticles affect the crosslinking of the elastomer chains, namely, disrupting the chains cross-linking while also anchoring the chains through the interphase. With the 4 vol. % nanocomposite, the swelling experimental results indicate that anchoring through the interphase is the dominant factor. The higher cross-linking density of the 4 vol. %

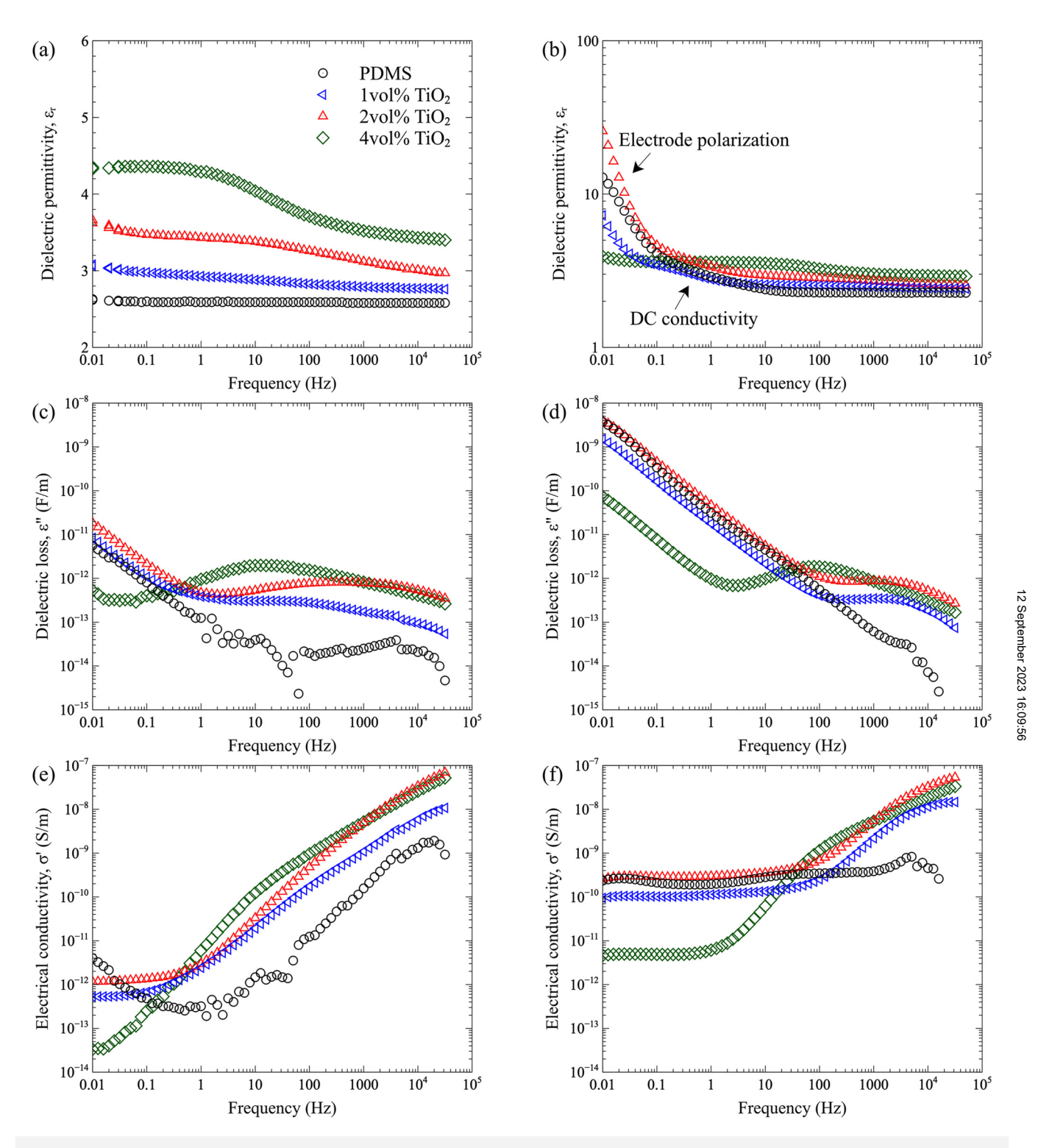


FIG. 1. Relative dielectric permittivity at (a) 25 and (b) 150 °C, dielectric loss at (c) 25 and (d) 150 °C, and electrical conductivity at (e) 25 and (f) 150 °C of PDMS, and 1, 2, and 4 vol. % TiO₂-PDMS nanocomposites.

TABLE I. The cross-linking density v and equilibrium degree of swelling Q of unfilled polydimethylsiloxane (PDMS) and the nanocomposites with 1, 2, and 4 vol. %

	PDMS	1 vol. %	2 vol. %	4 vol. %
Equilibrium degree of swelling, Q Cross-linking	1.98 ± 0.04	2.06 ± 0.06	2.18 ± 0.07	1.70 ± 0.02
density, v (10 ⁻⁵ mol/cm ³)	44 ± 2	40 ± 3	34 ± 3	74 ± 4

nanocomposite contributed to the charge suppression observed in the impedance spectroscopy results.

To further investigate the internal charge behaviors, the dc conductivity and TSDC spectra of the nanocomposites were analyzed and compared to unfilled PDMS. DC conductivities were extracted from the plateau of the electrical conductivity at low frequencies, and they are plotted as a function of temperature for unfilled PDMS and the TiO2-PDMS nanocomposites (Fig. 2). At 1 and 2 vol. % loadings, the dc conductivity did not significantly change compared to unfilled PDMS. The dc conductivity of the 4 vol. % nanocomposite was lower than unfilled PDMS by 1-2 orders of magnitude. The decrease in the dc conductivity and the suppression of the electrode polarization, which were most prominent in the 4 vol. % nanocomposite, can be attributed to the interphase dominating the effective properties due to its higher volume fraction compared to the lower contents. Plotting Ln (σ_{DC}) as a function of 1/T (Fig. S1 in the supplementary material) showed that the dc conductivity followed an Arrhenius behavior. Using Eq. (5), the activation energies of the dc conductivity, E_{DC} , for unfilled PDMS and the nanocomposites were extracted, and their values are summarized in Table II. The addition of the nanoparticles did not lead to statistically significant changes in the activation energy. We surmise that at low electric

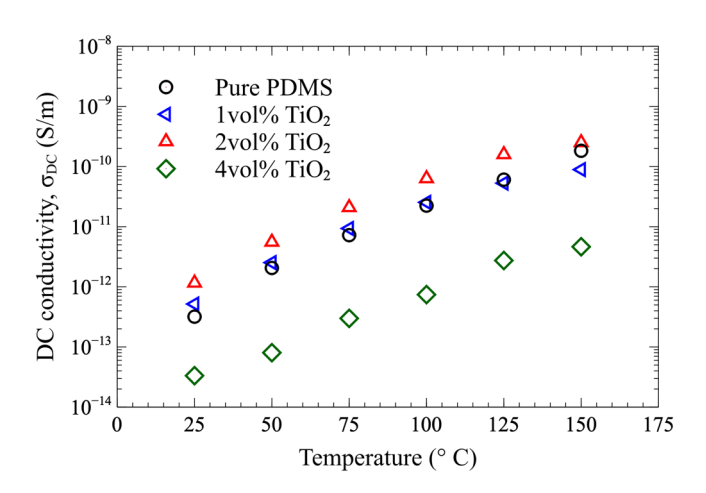


FIG. 2. DC conductivity of unfilled PDMS, and 1, 2, and 4 vol. % TiO2-PDMS nanocomposites as a function of temperature.

TABLE II. DC conductivity activation energy of the unfilled PDMS and the 1, 2, and 4 vol. % TiO2-PDMS nanocomposites.

	PDMS	1 vol. %	2 vol. %	4 vol. %
E_{DC} (eV)	0.53 ± 0.03	0.46 ± 0.03	0.48 ± 0.03	0.46 ± 0.03

fields, charges are detrapped and released at the same rate throughout the bulk of the elastomer matrix, and the changes in the conduction are governed by space charge movement through the material.³⁹ Therefore, the decrease in the dc conductivity is mainly due to the space charges being neutralized at the interphases—which are at a higher volume fraction with the 4 vol. % loading—and not due to a change in the charge trap depths, i.e., their activation energy,

$$\sigma_{DC} \propto \exp\left(-\frac{E_{DC}}{kT}\right).$$
 (5)

TSDC is a powerful technique to investigate the dielectric relaxations of polymers and polymer nanocomposites, as it has an excellent resolution because of its low equivalent frequency, usually below 1 mHz. Figure 3 shows the representative TSDC thermograms for unfilled PDMS and TiO2-PDMS nanocomposites, with 1, 2, and 4 vol. % loadings, after poling at 7.5 and 15 MV/m. The Bucci-Fieschi theory, which assumes a Debye single relaxation behavior, was used to analyze the peaks identified in the TSDC spectra and extract the activation energies. Common dielectric materials investigated using TSDC have multiple relaxations, and in order to use the Bucci-Fieschi model and extract activation energies for the different polarizations, the depolarization current density as a function of temperature, J(T), \vec{p} is decomposed into single peaks, and each peak is fitted to the following equation:

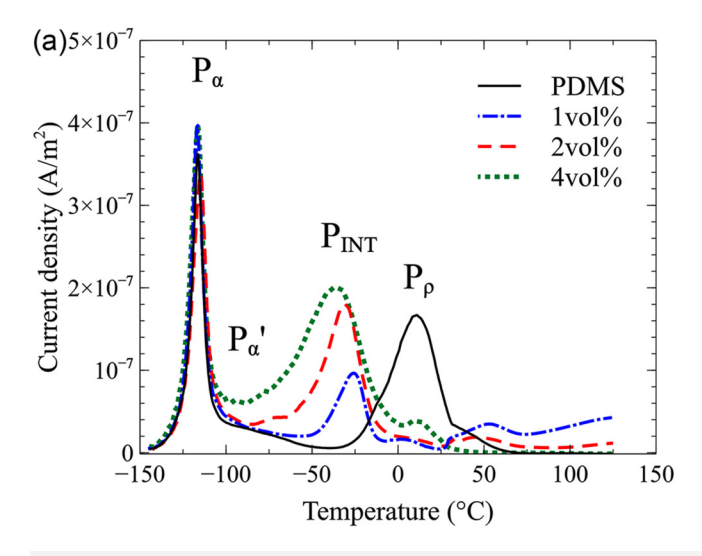
$$J(T) = \frac{P_o}{\tau_o} \exp\left(-\frac{E_a}{kT}\right) \exp\left[-\frac{1}{\beta \tau_o} \frac{kT^2}{E_a} \exp\left(-\frac{E_a}{kT}\right)\right], \quad (6)$$

where T is expressed in Kelvin, P_o is the equilibrium polarization reached at the poling temperature, E_a is the activation energy, k is the Boltzmann constant, β is the heating rate, and τ_o is the relaxation time at infinite temperature, which is calculated using the following equation:

$$\tau_o = \frac{kT_m^2}{\beta E_a} \exp\left(-\frac{E_a}{kT_m}\right),\tag{7}$$

where T_m is the temperature at which the current density reaches the maximum.

Table III lists the fitting results for the activation energy values (E_a) and the peak temperatures (T_m) for the different relaxations for all the samples after polarizing at 7.5 and 15 MV/m. The equivalent frequencies for the relaxations captured by TSDC were calculated using Eq. (8), and they ranged between 30 and $90 \mu Hz$,



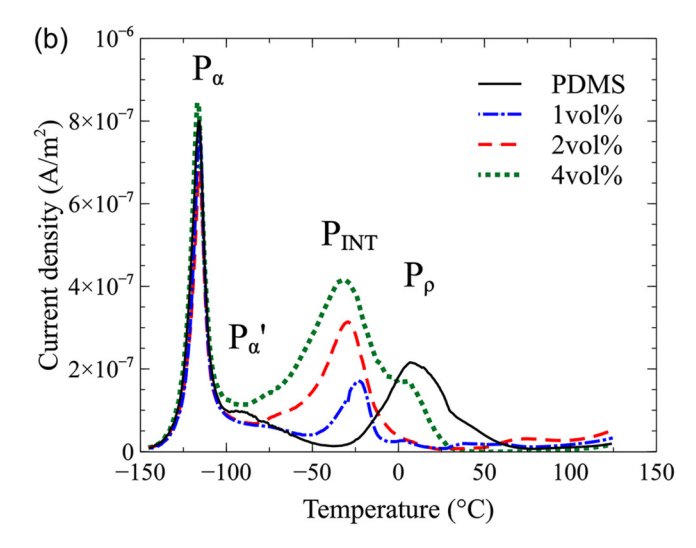


FIG. 3. Comparative TSDC thermograms for PDMS, and 1, 2, and 4 vol. % TiO₂-PDMS nanocomposites after poling at (a) 7.5 and (b) 15 MV/m.

$$f_{eq} = \frac{1}{2\pi} \frac{\beta E_a}{kT_m^2}.$$
 (8)

It is important to identify the origins of the relaxations thermally activated in the unfilled elastomer and the nanocomposites, whether it is dipolar polarization or space charges, to understand the fundamental electrical conduction mechanisms. When the polarizing field E_p is varied, the peak temperature of relaxation originating from dipolar polarization remains unaffected and its intensity varies proportionately with E_p . On the other hand, the space charge relaxation peak temperature depends on the polarizing field and their intensities have a non-linear dependence on The space charges can be due to intrinsic charges detrapped from the dielectric (heterocharge) or the injection of charge carriers from the electrode during the polarization step (homocharge). 46,47 When the space charges are thermally stimulated and they start moving, either (1) they would move toward the electrode with the opposite sign or (2) they are depleted by recombining with their counterparts within the dielectric.³⁹ Additionally, space charge relaxations occur at temperatures higher than those of dipolar orientation origins, since space charges would need to move over multiple atoms, while dipoles only require local rotation.

Space charge relaxations in polymers would occur above the glass transition temperature where an increase in the free volume facilitates the movement of the charges. The TSDC space charge relaxation in polymers is typically related to the electrical conductivity of the dielectric, with activation energy similar to that of the dc conductivity. The dielectrical properties of the different components would create an interfacial polarization, namely, the Maxwell–Wagner–Sillars (MWS) polarization. The different components would create an interfacial polarization, namely, the Maxwell–Wagner–Sillars (MWS) polarization. The different components would create an interfacial polarization, namely, the Maxwell–Wagner–Sillars (MWS) polarization.

As shown in Figs. 3(a) and 3(b), three distinct peaks were present in the TSDC spectra, and they will be referred to as P_{α} . $\stackrel{\smile}{8}$ $P_{\rm INT}$, and P_{ρ} from lower to higher temperatures. Some of the spectra have an additional peak between P_{α} and $P_{\rm INT}$; which will be referred to as P_{α} . With both polarizing fields, the first peak, P_{α} , is centered around -116 °C and is present in the depolarizing current spectra of all the samples. The narrow peak P_{α} is assigned to the segmental relaxation of the polymer backbone around the glass transition temperature (T_g) and is in good agreement with the literature for PDMS. $^{48-50}$ The activation energy for P_{α} ranged between 0.49 and 0.61 eV, with unfilled PDMS having the highest value, 0.61 eV. While the activation energy values of P_{α} decreased as the TiO₂ nanoparticle content increased, they were not affected by the

TABLE III. Activation energies and peak temperatures extracted from TSDC measurements for polarizing fields 7.5 and 15 MV/m corresponding to the three relaxations (the standard deviations ranged between 0.01 and 0.08 eV and 0–2.5 °C for E_a and T_m , respectively).

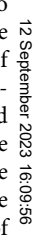
	P _α (7.5 15 MV/m)		P _{INT} (7.5 15 MV/m)		P _ρ (7.5 15 MV/m)	
	E _a (eV)	T _m (°C)	E _a (eV)	T _m (°C)	E _a (eV)	T _m (°C)
PDMS	0.59 0.61	-116 -116			0.48 0.48	9 7
1 vol. %	0.54 0.55	-116	0.56 0.55	-25 -23	•••	
2 vol. %	0.54 0.55	-116	0.41 0.38	-31 -30		
4 vol. %	0.49 0.51	-117	0.22 0.22	-34 -32	0.66 0.60	13 8

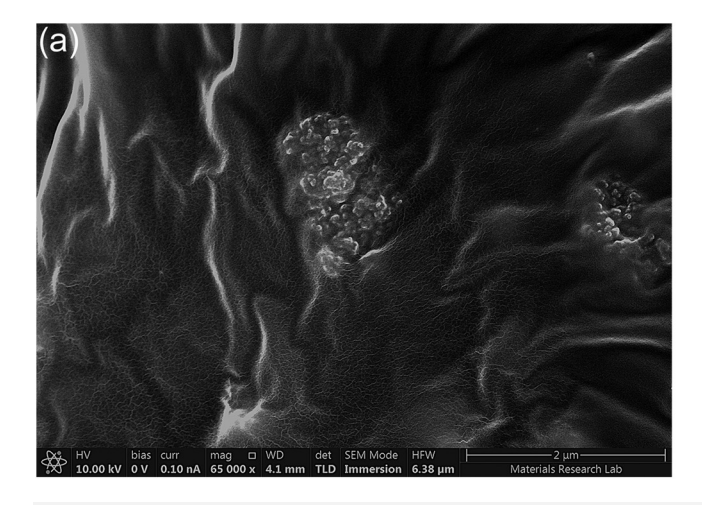
polarizing field. The intensity of P_{α} did not significantly change with the addition of the nanoparticles, and that is expected with the low contents investigated in this study. When the polarizing field was increased from 7.5 to 15 MV/m, the intensity of relaxation P_{α} in all the samples almost doubled, and the peak temperature remained unchanged, confirming its orientational origin due to the glass-to-rubber transition.

Above T_g the nanocomposites produced a depolarizing current peak, P_{INT}, between -70 and -10 °C, that was absent in the PDMS spectra under both poling conditions. Multiple observations indicate that P_{INT} is due to the TiO₂-PDMS interphase: (1) it was only present in the nanocomposites, (2) it appeared at a temperature higher than T_g because the interphase is more constrained by being bound to the particles and within the agglomerations, requiring a higher temperature than the bulk polymer chains (those far from the nanoparticles) to move and create relaxation, and (3) the intensity of the peak increased with the nanoparticles content, hence the interphase volume fraction. Scanning electron microscopy (SEM) images (Fig. 4) show the examples of TiO2 agglomerations, which consist of nanoparticles held together by thin layers of PDMS, bonded to the surrounding elastomeric matrix. Transmission electron microscopy (TEM) enables a closer look at the agglomerations as shown in Fig. 5. The TEM images illustrate a significant presence of the elastomer represented by the lighter regions between the darker nanoparticles within the agglomerations. The elastomer layers within and around the agglomerations make up the interphases that produce the P_{INT} depolarization currents. There are multiple potential contributors to the P_{INT} peak such as dipolar disorientations and space charges in the interphase.

With the addition of the TiO2 nanoparticles to PDMS, a hydrogen bond between Ti-O-H and Si-OH groups can form, and the creation of Si-O-Ti bonds is also possible, leading to an increase in polar groups in the nanocomposites.⁵¹ The presence of these polar groups might contribute to the depolarization currents of the nanocomposites. The contrast in the electrical properties of the TiO₂ nanoparticles and the PDMS matrix can lead to MWS polarization, leading to space-charge induced relaxation present only in the nanocomposites. The different relaxations originating from the presence of the interphase led to a distribution of relaxations encapsulated under a broad P_{INT} peak. Under both polarizing conditions, the P_{INT} peak became broader as the particles' volume fraction, i.e., the interphase volume fraction, increased. A small peak or "shoulder," P_{α} ', around $-75\,^{\circ}\text{C}$ appeared with $2\,\text{vol.}\,\%$ TiO2 loading while it was not identified with the 1 vol. % nanocomposite. With the 4 vol. % nanocomposite, the P_{α} and P_{INT} peaks are not clearly separated, resulting in the broadest interphase peak among the nanocomposites. The additional relaxation, P_{α} , can be associated with the elastomer chains around the agglomerates that are more constrained than bulk PDMS but looser than the chains bound to the nanoparticles and constrained within the agglomerates, leading to a relaxation temperature between the peak temperatures of P_{α} and P_{INT} . 19,20 It was not possible to extract clear peaks for $P_{\alpha}\mbox{'}$ relaxations in the different spectra; therefore, this relaxation was not fitted and was not included in Table III.

The third peak, P₀, appeared between −10 and 40 °C, with both polarizing fields. With 7.5 MV/m polarizing field, the intensity of P_o in the three nanocomposites is much smaller compared to unfilled PDMS. After polarizing at 15 MV/m electric field, the peak increased, especially for the 4 vol. % TiO₂-PDMS nanocomposite; yet, it remained lower than that of unfilled PDMS. For the 1 and 2 vol. % nanocomposites, the third relaxation remained practically suppressed. The maximum intensity of P_{ρ} was not proportional to the polarizing field, indicating the space charge origin: the maximum intensity remained nearly unchanged for the case of PDMS, while it quadrupled for the 4 vol. % TiO2-PDMS nanocomposite. Additionally, the peak temperature for both PDMS and 4vol. % TiO2-PDMS slightly shifted to lower temperatures as the polarizing field increased, which is consistent with a relaxation due of to the release of trapped charges in the dielectric bulk and/or at the interface with the electrodes (heterocharge). 46,52 The suppression of





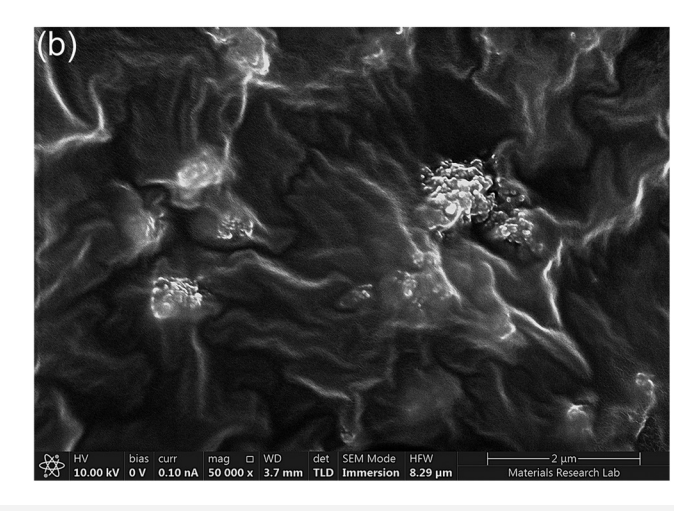
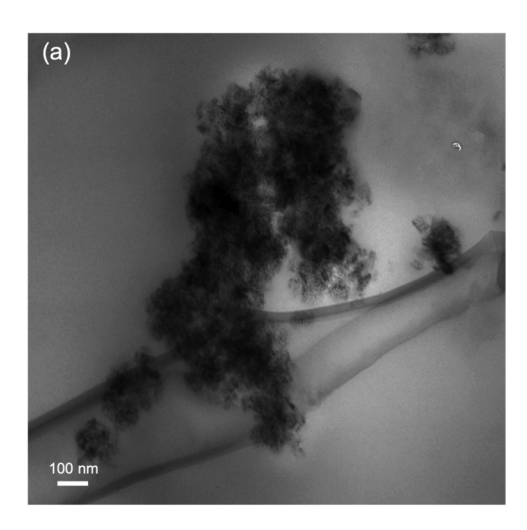


FIG. 4. Representative SEM images of agglomerations in the (a) 1 and (b) 4 vol. % nanocomposites, which consist of nanoparticles and occluded rubber encapsulated within the elastomer matrix.



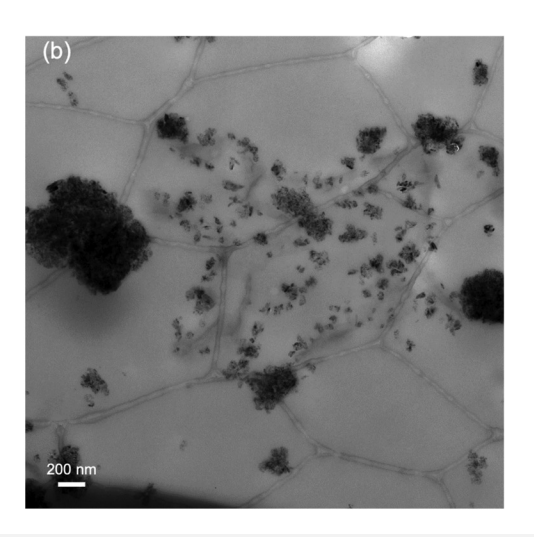


FIG. 5. Representative TEM images of agglomerations in the (a) 1 and (b) 4 vol. % nanocomposites. In these images, the lighter and darker regions correspond to the PDMS and TiO₂ nanoparticles, respectively.

the space charge relaxation in the nanocomposites with 1 and 2 vol. % loadings indicates that either (1) when thermally stimulated, the space charges were depleted by recombination with their counterparts possibly present around the particles, or (2) the trapped charges had deeper traps in these nanocomposites and were not released at this relaxation's temperature. The latter point can explain the increase in the depolarized currents seen about 50° C with the 1 and 2 vol. % nanocomposites. While at 4 vol. % loading, there are possibly more charge carriers with a distribution of trap depth compared to the 1 and 2 vol. %, leading to more charge detrapping and releasing, increasing the intensity of peak P_o. The activation energy of the 4 vol. % nanocomposite is slightly higher than that of unfilled PDMS, pointing to overall deeper traps in the nanocomposite. In addition, as mentioned in the dc conductivity discussion, the activation energies from dc conductivity and TSDC space charge relaxation are very similar in polymers,³⁵ which is the case for unfilled PDMS, where the calculated energies, E_{DC} and E_a (P_o), are 0.53 ± 0.03 and 0.48 ± 0.05 eV, respectively. A similar comparison was not done for the nanocomposites, since such a claim has not been established for heterogeneous systems. It was challenging to extract enough experimentally measured depolarized current for peak Pp for the 1 and 2 vol. % nanocomposites for an adequate fitting following Eq. (6). Therefore, their fitting parameters were not included in Table III.

IV. CONCLUSIONS

In this work, we investigated the effects of the interphase on the electrical behavior and relaxations of TiO2-PDMS nanocomposites with contents of 1, 2, and 4 vol. %. The combination of lowfield and low-frequency measurements confirms that the effects of the interphase on the electrical charges redistribution and mobility were most significant at 4 vol. % loading. At this content, there is a drastic reduction of the dielectric property dependence on the frequency and temperature, and a lowering of the dielectric losses

over a widening range of frequencies as temperature increases. To further identify the mechanism responsible for these differences, dc conductivity activation energies and TSDC spectra are analyzed; the 1-2 orders of magnitude reduction in dc conductivity indicate the limited mobility of the charge carriers and suppression of the electrode polarization in the 4 vol. % loading, which can be related to redistribution and limited mobility of the charges throughout the nanocomposite due to the presence of the nanoparticles and the interphase surrounding them. We stipulate that the 4 vol. % exhibiting more charge suppression compared to the 2 vol. % nanocomposite is due to the bigger volume of the interphase, demonstrating that the interphase has a stronger effect on the internal charges than the nanoparticles themselves. The effects of the interphase on the electrical properties of the nanocomposites agree with the trend observed with the degree of cross-linking. After an initial decrease in the degree of cross-linking with the nanoparticles loading, an increase was measured for the 4 vol. % nanocomposite. The nanoparticle-polymer interphase strongly influences the nanocomposite behavior due to its significant volume when the particles are nano-sized, affording an opportunity to tune the dielectric response of the resulting nanocomposite. In this work, we have shown the significant impact of the interphase at very low loadings by employing a variety of techniques.

SUPPLEMENTARY MATERIAL

See the supplementary material for the Arrhenius plots of dc conductivity as a function of temperature for unfilled PDMS and TiO₂-PDMS nanocomposites.

ACKNOWLEDGMENTS

This work was supported by the National Science Foundation (NSF) through Award No. CMMI-1662720.

AUTHOR DECLARATIONS

Conflict of Interest

The authors have no conflicts to disclose.

Author Contributions

A. Barhoumi Meddeb: Formal analysis (equal); Funding acquisition (equal); Investigation (equal); Methodology (equal); Validation (equal); Visualization (equal); Writing – original draft (equal); Writing – review & editing (equal). Z. Ounaies: Formal analysis (equal); Funding acquisition (equal); Investigation (equal); Methodology (equal); Validation (equal); Visualization (equal); Writing – original draft (equal); Writing – review & editing (equal).

DATA AVAILABILITY

The data that support the findings of this study are available from the corresponding author upon reasonable request.

REFERENCES

- ¹S. Zhao, L. Schadler, R. Duncan, H. Hillborg, and T. Auletta, Compos. Sci. Technol. **68**, 2965 (2008).
- ²T. Sun, Y. Wang, Y. Yang, H. Fan, M. Liu, and Z. Wu, Compos. Sci. Technol. 193, 108146 (2020).
- ³F. De Luca, G. Sernicola, M. S. P. Shaffer, and A. Bismarck, ACS Appl. Mater. Interfaces 10, 7352 (2018).
- ⁴Y. Shi, C. Liu, Z. Duan, B. Yu, M. Liu, and P. Song, Chem. Eng. J. **399**, 125829 (2020).
- ⁵F. Najafi, G. Wang, S. Mukherjee, T. Cui, T. Filleter, and C. V. Singh, Compos. Sci. Technol. **194**, 108140 (2020).
- ⁶H. A. I. Aziz, L. S. Nasrat, and R. M. El-Sharkawy, in 2017 International Conference on Electrical and Computing Technologies and Applications (ICECTA), Ras Al Khaimah, United Arab Emirates (IEEE, 2017), pp. 1–4.
- ⁷H. Li, F. Liu, H. Tian, C. Wang, Z. Guo, P. Liu, Z. Peng, and Q. Wang, Compos. Sci. Technol. 167, 539 (2018).
- ⁸T. Marinho, P. Costa, E. Lizundia, C. M. Costa, S. Corona-Galván, and S. Lanceros-Méndez, Compos. Sci. Technol. 183, 107804 (2019).
- ⁹B. Li, G. Polizos, and E. Manias, in *Dynamics of Composite Materials*, edited by A. Schönhals and P. Szymoniak (Springer International Publishing, Cham, 2022), pp. 225–249.
- H. Luo, X. Zhou, C. Ellingford, Y. Zhang, S. Chen, K. Zhou, D. Zhang,
 C. R. Bowen, and C. Wan, Chem. Soc. Rev. 48, 4424 (2019).
- ¹¹P. K. Singh, P. Goyal, A. Sharma, Rajesh, D. Kaur, and M. S. Gaur, Polym. Bull. 75, 4003 (2018).
- ¹²A. N. Asokan, A. P. Anagha, P. Preetha, and K. Sunitha, IEEE Trans. Dielectr. Electr. Insul. 26, 1211 (2019).
- ¹³A. N. Netravali and K. L. Mittal, Interface/Interphase in Polymer Nanocomposites (John Wiley & Sons, Incorporated, Somerset, 2016).
- ¹⁴B. Carroll, S. Cheng, and A. P. Sokolov, Macromolecules 50, 6149 (2017).
- ¹⁵C. Li, J. Evans, N. Wang, T. Guo, and S. He, Sci. Rep. **9**, 11290 (2019).
- ¹⁶R. Sanchez-Hidalgo, C. Blanco, R. Menendez, R. Verdejo, and M. A. Lopez-Manchado, Polymers 11, 449 (2019).
- ¹⁷E. Helal, L. G. Amurin, D. J. Carastan, R. R. de Sousa, Jr., E. David, M. Fréchette, and N. R. Demarquette, Polym. Eng. Sci. 58, E174 (2018).
- ¹⁸I. Sulym, P. Klonos, M. Borysenko, P. Pissis, and V. M. Gun'ko, J. Appl. Polym. Sci. **131**, 4154 (2014).
- ¹⁹P. Klonos, A. Panagopoulou, A. Kyritsis, L. Bokobza, and P. Pissis, J. Non-Cryst. Solids 357, 610 (2011).

- ²⁰P. Klonos, C. Pandis, S. Kripotou, A. Kyritsis, and P. Pissis, IEEE Trans. Dielectr. Electr. Insul. 19, 1283 (2012).
- ²¹J. Choi, H. Shin, S. Yang, and M. Cho, Compos. Struct. 119, 365 (2015).
- ²²D. Hou, J. Yu, and P. Wang, Compos. Part B: Eng. 162, 433 (2019).
- ²³ A.-C. Genix, V. Bocharova, B. Carroll, P. Dieudonné-George, E. Chauveau, A. P. Sokolov, and J. Oberdisse, ACS Appl. Mater. Interfaces 15, 7496 (2023).
- ²⁴Y. Liu, T. Yang, B. Zhang, T. Williams, Y.-T. Lin, L. Li, Y. Zhou, W. Lu, S. H. Kim, L.-Q. Chen, J. Bernholc, and Q. Wang, Adv. Mater. 32, 2005431 (2020)
- ²⁵O. Lopez-Pamies, T. Goudarzi, A. B. Meddeb, and Z. Ounaies, Appl. Phys. Lett. **104**, 242904 (2014).
- 26A. B. Meddeb, T. Tighe, Z. Ounaies, and O. Lopez-Pamies, Compos. Part B: Eng. 156, 166 (2019).
- ²⁷J. Shao, X. Liu, and M. Ji, J. Appl. Polym. Sci. 139, 51604 (2022).
- ²⁸L. O. Prasad, S. S. Pillai, and S. Sambandan, in 2019 IEEE International Conference on Flexible and Printable Sensors and Systems (FLEPS) (IEEE, 2019), pp. 1-3.
- pp. 1-3. ²⁹F. Klug, S. Solano-Arana, N. J. Hoffmann, and H. F. Schlaak, Smart Mater. Struct. 28, 104004 (2019).
- ³⁰P. Wang, L. Yang, B. Dai, Z. Yang, S. Guo, G. Gao, L. Xu, M. Sun, K. Yao, and J. Zhu, Eur. Polym. J. 123, 109382 (2020).
- ³¹T. Rehman, M. Nafea, A. A. Faudzi, T. Saleh, and M. S. M. Ali, Smart Mater. Struct. **28**, 115044 (2019).
- ³²M. Malekshahi Byranvand, A. Nemati Kharat, L. Fatholahi, and Z. Malekshahi Beiranvand, J. Nanostruct. 3, 1 (2013).
- ³³A. J. Haider, Z. N. Jameel, and I. H. M. Al-Hussaini, Energy Procedia 157, 17 (2019).
- ³⁴J. Schweitzer, S. Merad, G. Schrodj, F. Bally-Le Gall, and L. Vonna, J. Chem. Educ. 96, 1472 (2019).
- 35W. Chassé, M. Lang, J.-U. Sommer, and K. Saalwächter, Macromolecules 45, 899 (2012)
- **36**F. Kremer and A. Schönhals, *Broadband Dielectric Spectroscopy* (Springer, Berlin, 2003).
- 37 A. A. Skordos and I. K. Partridge, J. Polym. Sci., Part B: Polym. Phys. 42, 146
- ³⁸J. Mijović, S. Andjelic, B. Fitz, W. Zurawsky, I. Mondragon, F. Bellucci, and L. Nicolais, J. Polym. Sci., Part B: Polym. Phys. 34, 379 (1996).
- 39J. van Turnhout, in *Electrets*, edited by G. M. Sessler (Springer, Berlin, 1987), 50 np. 81–215
- pp. 81–215.

 40 J. Gasiot and J. Vanderschueren, in *Topics in Applied Physics*, edited by P. Bräunlich (Springer, Berlin, 1979), pp. 135–223.
- ⁴¹F. Namouchi, W. Jilani, and H. Guermazi, J. Non-Cryst. Solids **427**, 76 (2015).
- ⁴²Q. Zhang, Y. Zhang, X. Liu, X. Song, J. Zhu, and I. Baturin, J. Electron. Mater. 45, 4044 (2016).
- ⁴³M. Gaur, P. Shukla, R. Tiwari, A. Tanwar, and S. P. Singh, Indian J. Pure Appl. Phys. 46(8), 535–539 (2008).
- ⁴⁴A. A. Alagiriswamy, K. S. Narayan, and G. Raju, J. Phys. D: Appl. Phys. 35, 2850 (2002).
- ⁴⁵C. Lavergne and C. Lacabanne, *Electrical Insulation Magazine* (IEEE, 1993), Vol. 9, p. 5.
- 46 V. V. R. N. Rao, K. J. Krishna, and B. S. Rao, Acta Polym. 43, 68 (1992).
- ⁴⁷S. H. Carr, Electrical Properties of Polymers (Academic Press, New York, 1982), pp. 215–239.
- 48 A. E. Özçam, K. Efimenko, and J. Genzer, Polymer 55, 3107 (2014).
- ⁴⁹D. Fragiadakis, L. Bokobza, and P. Pissis, Polymer **52**, 3175 (2011).
- 50 P. Klonos, A. Panagopoulou, L. Bokobza, A. Kyritsis, V. Peoglos, and P. Pissis, Polymer 51, 5490 (2010).
- 51 S. S. Madaeni, M. M. S. Badieh, V. Vatanpour, and N. Ghaemi, Polym. Eng. Sci. 52, 2664 (2012).
- 52T. N. M. Ngo, U. Adem, and T. T. M. Palstra, Appl. Phys. Lett. 106, 152904 (2015)